Experimental parametric investigation on the behavior of adhesively bonded CFRP/steel joints

Anis Mohabeddine [a,b,*], Ghassan Malik [c], José Correia [b,d], Filipe Silva [d], Abílio De Jesus [e], Nicholas Fantuzzi [c], José Miguel Castro [b]

[a] Faculty of Civil Engineering and Geosciences, Delft University of Technology, Netherlands
[b] CONSTRUCT, Faculty of Engineering, University of Porto, 4200-465 Porto, Portugal
[c] DICAM – Department, School of Engineering and Architecture, University of Bologna, Italy
[d] INEGI, Institute of Science and Innovation in Mechanical and Industrial Engineering, 4200-465 Porto, Portugal
[e] Faculty of Engineering, University of Porto, 4200-465 Porto, Portugal

A B S T R A C T

This paper presents an extensive experimental and numerical study on the behavior of CFRP/Steel adhesively bonded double strap joints (DSJ). A total of 50 DSJ specimens were tested under static tensile loading. The digital image correlation (DIC) was used to measure the backface deformation. A total of six adhesives that feature different stiffness, strength, ductility, and toughness were analyzed. A parametric study including several variants was carried out. The influencing parameters considered are the following: the adhesive type, adhesive thickness, CFRP elastic modulus, CFRP length, surface treatment, and steel thickness. The results revealed that rigid adhesives commonly used in the construction industry do not provide the best performance for the CFRP/steel joints, instead, tough adhesives which combine high strength and ductility are more suitable for strengthening metallic infrastructures. Steel plastic yielding has a significant influence on the strength, behavior, and failure modes of the CFRP/steel adhesive joint. A numerical model validated with experimental data was developed in ABAQUS. The experimental observations including failure modes, joint strengths, and ductility were discussed using the numerical model. The joint strength efficiency is highly recommended as a design criterion for bonded joints.

1. Introduction

The repair of aging metallic infrastructures is a worldwide issue [1,2]. A large number of bridges in Europe, USA, and Japan has more than 100 years old and face problems of aging such as fatigue and corrosion that require particular attention [3–5]. The replacement of these structures is economically unfeasible. Therefore, the development of effective repair solutions is of paramount interest. The application of bonded carbon fiber reinforced polymers (CFRP) patches to repair deficient metallic structural elements is a judicious repair solution with a great potential for strengthening aging metallic infrastructures. The CFRP can reduce the stresses in the metallic structural elements without altering their original mechanical and fatigue properties as in the case of traditional repair methods that involve drilling or welding. This repair technology is well established in the aeronautical industry for more than

three decades [6], where a bonded composite patch is commonly applied to the defected/cracked area. However, for strengthening metallic infrastructures, this technology is still in its early stages.

Considerable research studies focused on the characterization of the behavior of CFRP/Steel adhesive joints [7–11] investigating several factors that can influence the performance, among them are: the surface preparation of the adherends [7,11,12], the stiffness of the CFRP [14], mechanical properties of the adhesive [7,15,16], the thickness of the adhesive layer [7,17], and the bond length [18–20]. However, most studies in the literature used brittle adhesives which were developed initially for concrete structures. Although these brittle adhesives can bond well to steel substrates, they may not provide the best performance for metallic structures. Yu et al. [7] compared Steel/CFRP joints with different adhesives. Joints with Araldite 420A/B (a ductile adhesive) achieved significantly higher strength than the brittle ones, however,

these joints failed under delamination failure mode, which is usually undesired by researchers in the literature [7,21]. Hence, the authors [7] did not consider joints with ductile adhesive for the derivation of the design rules. The traditionally desired cohesive failure becomes almost unachievable when tough adhesives are used. The ubiquitous empirical bond-slip models adopted in civil engineering-related research are only limited to cohesive failure [8] and little is known about other failure modes such as the CFRP delamination [22].

The mechanical properties of the adhesive have a significant influence on the performance of the steel/CFRP adhesive joints. Recent tough adhesives with high strength and ductility are more appropriate for bonding metallic substrates [23]. Very recently, SIKA® [24] developed a moderately tough adhesive (i.e. Sikadure 370) for the repair of steel bridges affirming that the highly brittle 2C-epoxy adhesives used in construction practice are suitable for concrete and other cementitious systems but for more ductile substrates such as steel, toughened ductile adhesives should be used. Kasper et al. [2] characterized the behavior of the Sikadure 370 and compared it with the most common brittle adhesive used in the related research (Sikadure 30). The results revealed that the more ductile adhesive Sikadure 370 is more suitable for the strengthening of steel bridges due to its high strength and durability.

Previous research studies [7–9,13,15,16,18–20,25] that focused on the characterization of CFRP/steel bonded joints designed their specimens in order to avoid yielding in the steel part, which reasonable if the objective is to characterize the shear behavior of the adhesive in a bonded joint. However, in old metallic riveted bridges, the thickness can be as low as 5 mm [26] and the yielding strength of a structural detail reinforced with a composite patch can be reached at relatively low applied forces especially since the composite patch does not share dead load stresses. Yielding in the base material should influence the behavior significantly. To the best knowledge of the authors, there are no studies that included this issue. So, it is important to use more representative steel sections and examine their behavior if yielding is reached.

This paper presents an experimental and numerical study on the behavior of adhesively bonded Steel/CFRP joints. Firstly, experimental coupon tests on several adhesive types are conducted to compare their basic mechanical properties. Then, adhesively bonded CFRP/steel double strap joints, representative of a composite patch repair over the cracked region [27,28], are tested under static tensile loading. Several variants are investigated including the influence of the adhesive type, CFRP stiffness, surface preparation, CFRP length, and steel thickness. The digital image correlation (DIC) is used to measure the deformation on the back face of the CFRP. A continuum finite element model calibrated with experimental data is developed in ABAQUS. Based on the experimental and numerical results a comprehensive discussion on the behavior and the design of steel/CFRP joints is provided.

2. Experimental program

2.1. Materials

2.1.1. Adhesives

A total of 6 six different adhesives were selected for testing. Dog-bone specimens were manufactured and tested under tensile loading to compare the behavior of the different adhesives. The specimens were designed according to ASTM D638-14 [29] category 5 which is recommended for the comparison between different adhesive types. The adhesives consist of:

- **Sikadur 30. (SK-30):** an epoxy-based linear brittle adhesive used in the construction industry and the most common adhesive used research studies related to steel/CFRP joints.
- **S&P HP220:** an epoxy-based linear rigid adhesive commonly used in the construction industry.

- **Sika Power 1277 (SK-P):** an epoxy-based ductile adhesive developed for the automotive industry but can be found in the research literature for steel structures.
- **Araldite 2052–1. (AR):** an acrylic-based ductile adhesive developed for harsh environments. It has high resistance to humidity and high temperature. The manufacturers claim that it requires no or limited surface preparation.
- **Araldite AW4858/HW4858. (AW):** An epoxy-based ductile adhesive developed for different mechanical engineering industries. It has high peeling resistance and shear resistance.
- **Araldite LY5052/Aradur 5052CH. (LY):** an epoxy-based linear adhesive developed for CFRP impregnation and wet-layup technique.

The specimens were manufactured using an acrylic mould covered with flat rectangular acrylic plates and compressed with weights to ensure constant thickness. The specimens were left to cure for at least 7 days at room temperature. The adhesive specimens were tested in MTS 831–02 Elastomer test system, as shown in Fig. 1. The strain measurements were taken using clip gauges. The specimens were subjected to static tensile loading until complete failure. The speed of the loading was 1 mm/minute except for very brittle adhesives (SIKADUR 30) that failed before one minute, the speed was reduced to 0.5 mm/minute. Since the ASTM D638 recommends using a speed between 0.5 and 5 mm/minute given that the duration of the test shall be more than 1 min.

The basic average material properties of the adhesives are presented in Table 1, including the Young's modulus, the maximum stress, maximum deformation at failure, and toughness which is measured as the area under the stress–strain curve. Fig. 2 illustrates the stress–strain curves of the different adhesives. The adhesive SK30 reached high strength (i.e. 35MPa) and stiffness but very low strain capacity up to 0.3 %. The adhesive S&P HP220 has a lower stiffness than SK30 and reaches roughly similar strength but with a double deformation capacity compared to SK30. The adhesive LY has an intermediate rigidity and very high strength with an average maximum of 57.6MPa. The ductile adhesives AW, AR, and SK-P exhibit a lower stiffness than the rigid adhesives. The adhesive AW reached a high strength of 35MPa and significantly longer deformation at failure with an average factor of
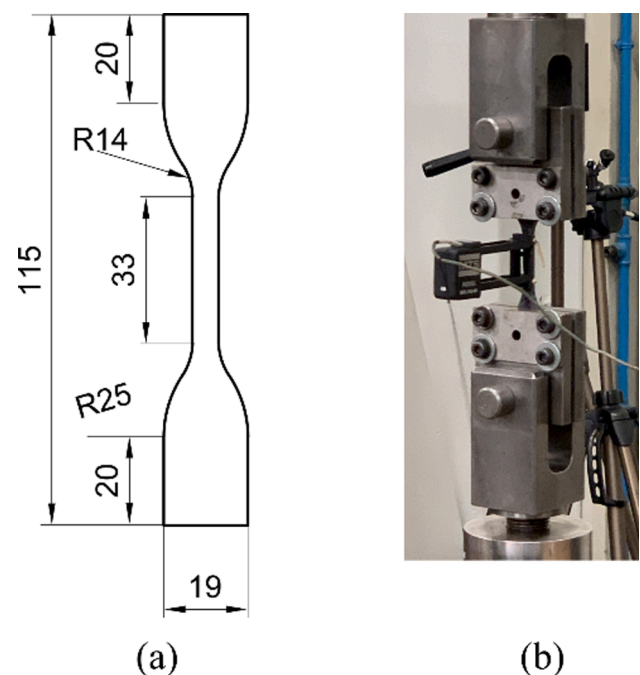

Fig. 1. Adhesive dog-bone tensile test in MTS 831–02: a) specimen geometry (in mm); b) experimental test setup.

Table 1
Adhesives' average mechanical properties.

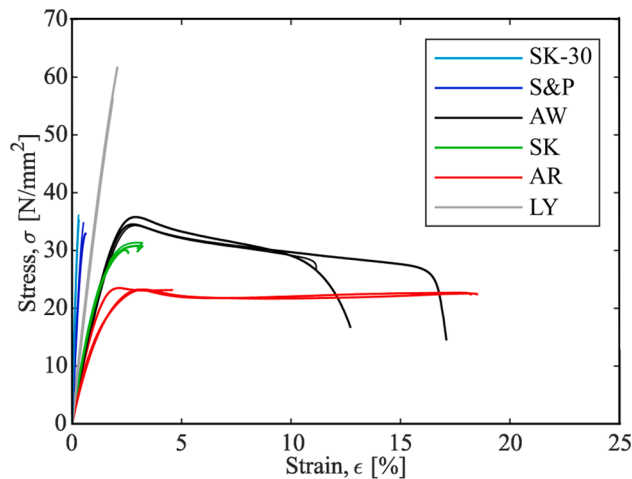| Adhesive	E (MPa)	Max stress (MPa)	Max Deformation (%)	Toughness ($N.mm.mm^{-3}$)
SK-30	12,915	35.03	0.28	0.058
HP220	7600	33.16	0.54	0.108
AW	1350	34.9	13.6	3.9
AR	1240	23.3	18.4	3.88
LY	3255	57.6	1.9	0.59
SK	1695	30.8	2.97	0.64

Fig. 2. Stress–strain curves of adhesive dog-bone tensile tests.

13.6 %. The adhesive SK-P reached an average strength of $30.8 MPa$ but did not exhibit large plastic deformation. The adhesive AR reached the lowest strength with the value of $23.3 MPa$ but the largest deformation capacity up to 18.4%. Note one specimen with AR adhesive failed prematurely, as shown in Fig. 2, it was excluded from the calculation of the average mechanical properties. The premature failure was mainly due to a large void that was found inside the material in the failed section.

2.1.2. CFRP

Two types of CFRP were used in this study: (a) prefabricated pultruded unidirectional laminates (i.e. S&P reinforcement HM (200/2000) and SIKA Carbodure S512 where both of them are made with fiber volume content >68 % according to their datasheets provided by the manufacturers, see [31] and [30], respectively; and (b) high modulus CFRP sheets (S&P C-Sheet 640) that were impregnated with the adhesive by the authors in the lab using the wet layup technique. The Araldite LY5052/Aradur 5052CH (LY) was used for the impregnation of the CFRP sheets. The fiber content was 65 % in volume. Two methodologies were applied in the wet layup technique which consists of:

Method 1: Impregnating the CFRP sheets with the adhesive LY5052/Aradur 5052CH during the manufacture of the CFRP/Steel double strap joint. In this case, the adhesive (LY) is used to wet the CFRP sheets and to bond the CFRP with the steel bars. This technique is commonly used in the literature.

Method 2: Prefabricating the CFRP laminates using the vacuum bagging technique. Once cured, the CFRP laminates were cut to the required dimensions. In this case, any adhesive can be used to bond the CFRP/steel adhesive joint as the CFRP is prefabricated.

The mechanical properties of the CFRP provided by the manufacturer are presented in Table 2.

2.1.3. Steel

Steel bars made with two thicknesses (i.e. 6 mm and 10 mm) made of European hot rolled carbon steel S275 were used in this study. The

Table 2
Basic manufacturer's mechanical and geometrical properties of the CFRP.

Type	Young modulus (GPa)	Ultimate stress (MPa)	Elongation at break (%)	Thickness (mm)
S&P HM 200/2000	205	2800	1.3 %	1.4
SIKA Carbodure S512	170	1700	1.8 %	1.2
S&P C-Sheet 640	640	2600	0.4 %	0.168

measured mechanical properties are shown in Table 3.

2.2. Manufacture of double strap joints specimens

Adhesively bonded CFRP/Steel double strap joint specimens (DSJ) are used to assess the behavior of the adhesive interface between steel and CFRP. DSJ specimens are commonly adopted since they are representative of a composite patch repair over a cracked region [27,28]. A typical double strap joint, as shown in Fig. 3, is constituted by two separate steel bars joint together with a bonded CFRP patch on both sides.

The manufacture of the specimens involved mainly-two steps:

(a) Surface preparation of the steel and CFRP:

The surface preparation is a key step for the successful bonding of structural adhesives [32]. Except for two specimens that had the surface treated only with sandpaper grit 80 using an angle grinder, all the specimens had the steel substrates sandblasted. The alumina dioxide sand F60 with grain size between $212 - 300 microns$ was used to prepare the surface of the joint, as recommended in [12] to avoid adhesion failure in the steel-adhesive interface which usually occurs due to inadequate surface preparation. Once the specimens were polished, the surfaces were cleaned with compressed air and acetone to remove any oil or particles left from the surface preparation operation. The CFRP surface was polished with sandpaper grit 180 which is commonly used for composite materials. The polishing of the CFRP plates was made carefully and only in the direction of the fibers.

(b) Application of the adhesive bonding between CFRP and steel in the mould:

The double strap joints were manufactured using aluminium moulds that have been fabricated at the Department of Mechanical Engineering (DEMEC) workshop in the Faculty of Engineering of the University of Porto (FEUP). The moulds are made of two flat aluminium plates of 25 mm thickness, 1300 mm long, and 250 mm width. The moulds can accommodate 4 specimens in the longitudinal direction separated by pins to ensure that the CFRP and the steel bars are well aligned. The preparation of the mould includes cleaning and applying the unmoulding agent to be able to unmould the specimens after curing. The adhesives were applied on both CFRP, and the steel then bonded together. Once, the CFRP and the steel bars were joined together, aluminium spacers were used to maintain the predefined adhesive thickness constant after closing the mould where the upper mould plate

Table 3
Measured mechanical properties of S275.

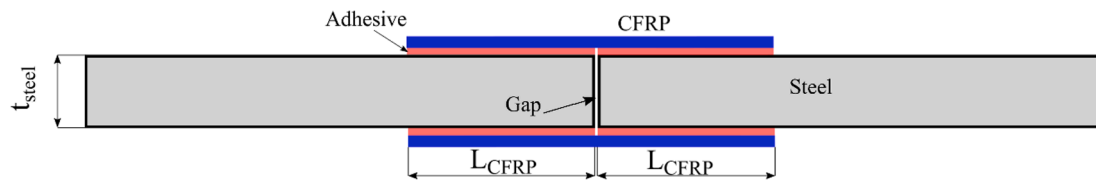| Material	Yield stress (MPa)	Ultimate stress (MPa)	Elastic modulus (GPa)
S275 (10 mm)	350	439	200
S275 (6 mm)	324	458	200

Fig. 3. Schematic view of double strap joint specimens.

will apply uniform pressure on the specimens. Then, the specimens were left to cure for at least 7 days at room temperature.

2.3. Experimental setup

The double strap joint specimens were tested in an ESH testing machine as shown in Fig. 4. The specimens were subjected to static tensile loading until complete failure. The loading speed was 1 mm/minute. The strain fields on the back face of the CFRP plates or the lateral face of the joint were captured using 2D digital image correlation (DIC). A random speckle pattern with a black background and white spots was applied on the back face of the CFRP. Note, that a maximum of 100 mm lens imaging was used so the lenses were controlled to achieve a sharp focus only on half of the joint.

2.4. Experimental testing matrix

A total of 50 DSJ specimens have been tested, the experimental matrix is presented in Table 4. The nomenclature of each specimen is given as follows "DSJ-CFRP name- CFRP length - Steel thickness -Adhesive name - Adhesive thickness- repetition No". Two specimens include (AG) at the end which refers to surface preparation with angle grinding. The pultruded CFRP S&P HM 200/2000 and CARBODUR S512

Fig. 4. Experimental setup.

are presented as (S&P) and S512, respectively. The acronyms H10 and H5 stand for CFRP laminates impregnated using vacuum bagging technique with 10 layers and 5 layers of high modulus CFRP sheets S&P/$C^{-640}(-|-)$, respectively. Whereas, WH5 and WH1 stand for 5 layers and 1 layer of high modulus S&P/$C^{-640}(-|-)$ CFRP sheets applied directly on the specimens using the wet layup technique. The abbreviations for failure modes are as following: A: Adhesive failure; C: Cohesive failure; D: Delamination mode of Failure; R: CFRP rupture. Note: for combined failure modes, the first letter is the dominant failure mode.

3. Experimental results

3.1. Load displacement curves

Fig. 5 (a) illustrates the load–displacement curves for specimens "DSJ-SP–75–10-AW-repetition No." which are made by the tough adhesive AW4858/HW4858 (1mm thickness), normal modulus CFRP (S&P $L = 75mm$), and a steel thickness of 10 mm. The maximum loads reached are between 150KN and 170KN, which is very close to the yield strength of the steel bar, as shown in the figure where a load–displacement curve of a bare steel bar of the same material and geometry is plotted. Specimen "DSJ-SP–75–10-AW-6" shows a yielding flat plateau which indicates that the steel bar had yielded as will be discussed in the subsequent sections using numerical analysis. The maximum displacement reached before failure is 4.7mm. The limited ductility shown in the other repeated tests might be due to plastic deformations in the adhesive or steel yielding in regions of stress concentration which will be discussed further in the subsequent sections.

Fig. 5 (b) presents the load–displacement curves of 4 repeated DSJ specimens "DSJ-SP–75–10-SP-repetition No." bonded with S&P HP220 rigid adhesive. The specimens reached strength values between 99.9 −110kN, followed by an abrupt failure.

Fig. 5 (c) shows the load–displacement curves of 6 repeated tests of "DSJ-SP–75–10-SK30-1-(repetition No.)" which are made by the rigid adhesive SIKADUR30 (1 mm thickness), normal modulus CFRP (S&P), and a steel thickness of 10 mm. The strength reached values between 65 −85KN followed by a limited flat plateau in most cases. The flat plateau has been also reported in other studies in the literature [7] for joints with Sikadur 30. The maximum strength is associated with crack initiation in the middle of the joint and the flat plateau is attributed to the crack propagation which depends on the length of the bonded area.

Fig. 5 (d) illustrates the load–displacement curves for specimens with Araldite 2052–1 "DSJ-SP–75–10-AR-1-repetition No." which reached very high strength with values above 175kN except one which is considered as an outlier that reached only 156kN due large voids observed in the adhesive layer after failure. Specimen "DSJ-SP-75-10-AR-1–4" exhibits a large ductile plateau which follows the trend of the load–displacement curves of a bare steel bar as shown in the figure. The maximum displacement of 8.9mm was reached before failure which is almost double of the specimen "DSJ-SP–75–10-AW-6" made with AW4858/HW4858 adhesive that developed a ductile behavior.

Fig. 5 (e) and (f) present the load–displacement curves for specimens made with steel bars of $t_{steel} = 6mm$ for both the rigid adhesive S&P HP220 (i.e. DSJ-SP–75–6-SP-1-repetition No.) and the ductile adhesive AW4858/HW4858 (i.e. DSJ-SP–75–6-AW-1-repetition No.), respectively. Due to the lower yield strength of these steel bars (i.e. ≈ 100kN),

Table 4
Experimental testing matrix of steel/CFRP double strap joints.

No.	Specimen's Name	Control	Adhesive	Type of CFRP	$L_{CFRP}(mm)$	$t_{adhesive}(mm)$	$t_{steel}(mm)$	Strength (kN)	Failure mode
1	DSJ-SP-75-10-HP220-1-1	Adhesive type	HP220	S&P	75	1	10	103.8	D
2	DSJ-SP-75-10-HP220-1-2		HP220	S&P	75	1	10	99.9	D
3	DSJ-SP-75-10-HP220-1-3		HP220	S&P	75	1	10	110	D + C
4	DSJ-SP-75-10-HP220-1-4		HP220	S&P	75	1	10	106	D + C
5	DSJ-SP-75-10-AW-1-1		AW	S&P	75	1	10	155.5	D
6	DSJ-SP-75-10-AW-1-2		AW	S&P	75	1	10	161.5	D
7	DSJ-SP-75-10-AW-1-3		AW	S&P	75	1	10	168.6	D
8	DSJ-SP-75-10-AW-1-4		AW	S&P	75	1	10	153.0	D
9	DSJ-SP-75-10-AW-1-5		AW	S&P	75	1	10	161.0	D
10	DSJ-SP-75-10-AW-1-6		AW	S&P	75	1	10	166.9	D
11	DSJ-SP-75-10-SK30-1-1		SK30	S&P	75	1	10	80.0	C + D
12	DSJ-SP-75-10-SK30-1-2		SK30	S&P	75	1	10	80.0	C + D
13	DSJ-SP-75-10-SK30-1-3		SK30	S&P	75	1	10	76.6	C + D
14	DSJ-SP-75-10-SK30-1-4		SK30	S&P	75	1	10	70.8	C + D
15	DSJ-SP-75-10-SK30-1-5		SK30	S&P	75	1	10	66.7	C + D
16	DSJ-SP-75-10-SK30-1-6		SK30	S&P	75	1	10	82.1	C + D
17	DSJ-SP-75-10-AR-1-1		AR-52	S&P	75	1	10	156.2	D
18	DSJ-SP-75-10-AR-1-2		AR-52	S&P	75	1	10	177.5	D
19	DSJ-SP-75-10-AR-1-3 (AG)		AR-52	S&P	75	1	10	175.1	D
20	DSJ-SP-75-10-AR-1-4 (AG)		AR-52	S&P	75	1	10	175.3	D
21	DSJ-SP-75-10-AW-0.6-1	Adhesive thickness	AW	S&P	75	0.6	10	174.4	D
22	DSJ-SP-75-10-AW-0.6-2		AW	S&P	75	0.6	10	174.3	D
23	DSJ-SP-75-10-AW-1.6-1		AW	S&P	75	1.6	10	142.5	D
24	DSJ-SP-75-10-HP220-0.6-1		HP220	S&P	75	0.6	10	122.0	C + D
25	DSJ-SP-75-10-HP220-1.6-1		HP220	S&P	75	1.6	10	117.3	C + D
26	DSJ-SP-75-10-HP220-0.6-2		HP220	S&P	75	0.6	10	122.0	C + D
27	DSJ-SP-75-10-HP220-1.6-2		HP220	S&P	75	1.6	10	109.7	D + C
28	DSJ-SP-75-6-AW-1-1	Steel thickness	AW	S&P	75	1	6	121.5	D
29	DSJ-SP-75-6-AW-1-2		AW	S&P	75	1	6	107.9	D
30	DSJ-SP-75-6-AW-1-3		AW	S&P	75	1	6	119.8	D
31	DSJ-SP-75-6-AW-1-4		AW	S&P	75	1	6	105.4	D
32	DSJ-SP-75-6-HP220-1-1		HP220	S&P	75	1	6	101.4	A + D
33	DSJ-SP-75-6-HP220-1-2		HP220	S&P	75	1	6	105.2	A + D
34	DSJ-SP-75-6-HP220-1-3		HP220	S&P	75	1	6	101.9	A + D
35	DSJ-SP-75-6-HP220-1-4		HP220	S&P	75	1	6	101.0	A + D
36	DSJ-SP-30-10-AW-1-1	CFRP length	AW	S&P	30	1	10	72.5	D
37	DSJ-SP-50-10-AW-1-2		AW	S&P	50	1	10	104.4	D
38	DSJ-SP-30-10-HP220-1-1		HP220	S&P	30	1	10	39.1	C + D
39	DSJ-SP-30-10-HP220-1-2		HP220	S&P	30	1	10	35.3	C + D
40	DSJ-SP-50-10-HP220-1-1		HP220	S&P	50	1	10	76.9	D + C
41	DSJ-SP-50-10-HP220-1-2		HP220	S&P	50	1	10	85.9	D + A
42	DSJ-H10-75-6-AW-1-1	CFRP type	AW	H10	75	1	6	107.8	R
43	DSJ-H5-75-6-AW-1-1		AW	H5	75	1	6	115.7	R
44	DSJ-H5-75-6-AW-1-1		AW	H5	75	1	6	105.4	R
45	DSJ-W5-75-6-LY-1-1		LY	WH5	75	1	6	76.5	R
46	DSJ-W1-75-6-LY-1-1		LY	WH1	75	1	6	21.3	R
47	DSJ-H10-75-10-AW-1-1		AW	H10	75	1	10	161.3	R
48	DSJ-H10-75-10-AW-1-2		AW	H10	75	1	10	173.3	R
49	DSJ-SK-75-10-HP220-1-1		HP220	S512	75	1	10	119.6	A + D
50	DSJ-SK-75-10-HP220-1-2		HP220	S512	75	1	10	118.7	D + C

the DSJ specimens developed large plastic deformation before failure. Specimens made with the rigid adhesive SP HP220 "DSJ-SP-75–6-SP-1-repetition No." reached the yielding strength of the steel bars and developed ductile displacement up to 9.26mm. Whereas the specimens with the ductile AW4858/HW45858 developed much higher ductility and strain hardening. The maximum strength of the joint reached is 121kN and a maximum displacement of 33.6mm.

Fig. 5 (g) illustrates the specimens with the steel of $t_{steel} = 6mm$ bonded with high modulus CFRP laminates made using the wet-layup technique. As can be seen, specimens having the CFRP laminates made with vacuum bagging and bonded with AW4858/HW4858 adhesive (i.e. DSJ-H10-75–6-AW-1-1, DSJ-H5-75–6-AW-1-1, and DSJ-H5-75–6-AW-1–2) reached higher performance than the ones directly impregnated on the steel bars using LY5052/CH5052 epoxy resin (i.e. DSJ-W5-75–6-LY-1–1, DSJ-W1-75–6-LY-1–1). The specimens bonded AW4858/HW4858 reached the yield strength of the steel bars and developed some ductility and strain hardening. Whereas the specimens bonded with LY5052/CH5052 exhibited a linear behavior with a strength 76.5kN for DSJ-W5-75–6-LY-1–1 and 21.3kN for DSJ-W1-75–6-

LY-1–1. Note the latter specimen was made with only one layer of CFRP sheets (thickness 0.168mm) which justifies the lower strength reached.

Fig. 5 (f) shows the load–displacement curves of DSJ specimens made with the 10 layers of high modulus CFRP laminates "DSJ-H10-75–10-AW-1-repetition No." plotted with the ones made with pultruded CFRP S&P HM(200/2000) "DSJ-SP-75–10-AW-1-repetition No." for the sake of comparison. All the specimens are made with a steel thickness of 10mm and bonded with AW4858/HW4858. The specimens with high modulus CFRP reached high strength with values of 161.3kN and 173.3kN, which is comparable to the ones made with pultruded CFRP.

3.2. Failure modes

The failure modes and the inspection of the fracture surface provide important information on the behavior of the adhesive joint. According to Zhao and Zhang [33] and Majidi et al. [34] the possible mode of failure in the steel/CFRP joint are the followings: Adhesive failure at the adherents-adhesive interface caused usually by inadequate surface treatment [32], cohesive failure in the adhesive layer, CFRP rupture that
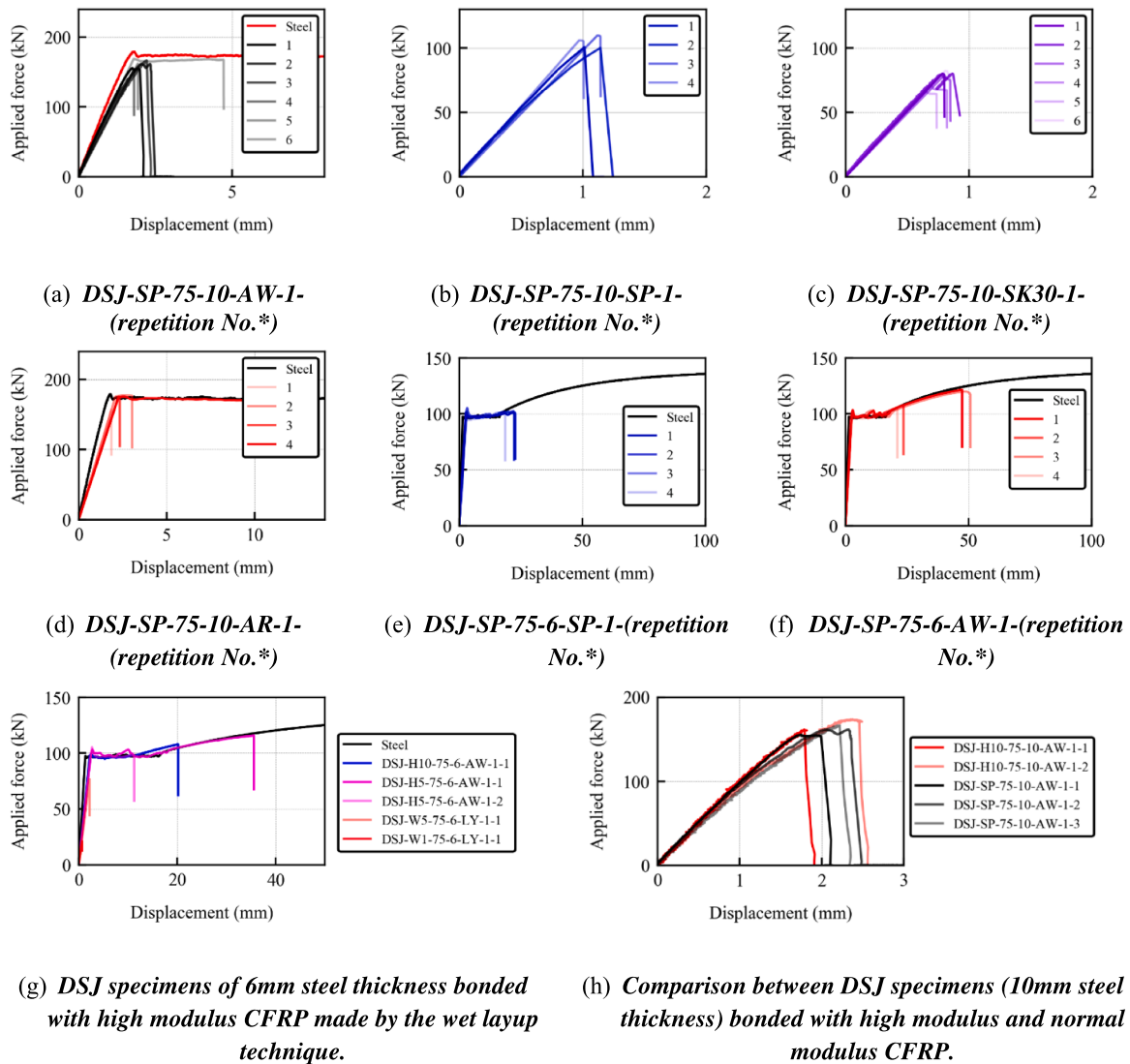
(a) *DSJ-SP-75-10-AW-1-(repetition No.*)*

(b) *DSJ-SP-75-10-SP-1-(repetition No.*)*

(c) *DSJ-SP-75-10-SK30-1-(repetition No.*)*

(d) *DSJ-SP-75-10-AR-1-(repetition No.*)*

(e) *DSJ-SP-75-6-SP-1-(repetition No.*)*

(f) *DSJ-SP-75-6-AW-1-(repetition No.*)*

(g) *DSJ specimens of 6mm steel thickness bonded with high modulus CFRP made by the wet layup technique.*

(h) *Comparison between DSJ specimens (10mm steel thickness) bonded with high modulus and normal modulus CFRP.*

Fig. 5. Double strap joints (DSJ) load–displacement curves (*Note that repetition No. is mentioned in the legend).

occurs for high modulus CFRP due to its limited deformation capacity [33], CFRP delamination, and steel yielding.

DSJ specimens made with pultruded CFRP and bonded with the tough adhesive AW4858/HW4858 failed under CFRP delamination failure mode, regardless of the adhesive thickness, the CFRP length, or the steel thickness (see Fig. 6 (a), (h), and (j)). This indicates the fracture toughness of the adhesive AW4858/HW4858 is higher than the fracture toughness of the CFRP matrix where the CFRP delamination occurs.

Fig. 6 (b) shows a typical failure mode of specimens bonded with SIKADUR30 adhesive which failed mainly under cohesive failure combined with limited delamination at the joint ends. This behavior has been also reported in previous studies which used SIKADUR30 [7]. This behavior indicates that SIKADUR30 has a lower fracture toughness than the CFRP delamination. The specimens with SIKADUR30 achieved the lowest strength compared to all other specimens.

Specimens made with steel bars of a thickness of 10 mm, pultruded CFRP, and bonded with S&P HP220 failed under CFRP delamination failure mode or a combination of cohesive and delamination, as shown in Fig. 6 (c) and (d).

Specimens made with pultruded CFRP and bonded with the ductile adhesive AR5052-1 failed mainly under CFRP delamination failure mode. Fig. 6 (e) and (f) show two specimens bonded by the adhesive AR5052-1 but had different steel surface treatments. The surface

treatment did not influence the failure mode of the specimens.

For specimens with shorter CFRP lengths (i.e. 30*mm* and 50*mm*), cohesive failure was more dominant than CFRP delamination for specimens made with S&P HP220 as shown in Fig. 6 (g).

For specimens with adhesive S&P HP220 and 6 mm of steel thickness, adhesive failure at the adhesive-steel interface and limited CFRP delamination governed the behavior, as shown in Fig. 6 (j). In these specimens, the steel bar experienced large plastic deformation as shown in Fig. 5, which changes the failure compared to the DSJ specimens that did not experience plasticity (i.e. $t_{steel} = 10mm$).

Fig. 6 (k) and (l) illustrate the failure mode of specimens made with high modulus CFRP made with the wet layup technique bonded with AW4858/HW4858 and LY5052/CH5052, respectively. Regardless of the adhesive type and the number of CFRP layers (i.e. Fig. 6 (k): 5 layers and Fig. 6 (l):1 layer), all specimens made with high modulus CFRP showed CFRP rupture mode of failure. The CFRP rupture failure mode occurs mainly due to the low deformation capacity of high modulus CFRP (i.e. 0.4 %). This observation in in line with the results of Chu et al. [11].

3.3. CFRP back face strain fields using DIC

Fig. 7 shows the strain field contour plots on the back face of the CFRP captured using DIC for DSJ specimens made with steel thickness

(a) DSJ-SP-75-10-AW-1-6

(b) DSJ-SP-75-10-SK30-1-5

(c) DSJ-SP-75-10-SP-0.6-2

(d) DSJ-SP-75-10-SP-1-1

(e) DSJ-SP-75-10-AR-1-3 (AG)

(f) DSJ-SP-75-10-AR-1-2

(g) DSJ-SP-30-10-SP-1-1

(h) DSJ-SP-30-10-AW-1-1

(i) DSJ-SP-75-6-SP-1-1

(j) DSJ-SP-75-6-AW-1-2

(k) DSJ-W1-75-6-LY-1-1

(l) DSJ-W1-75-6-LY-1-1

Fig. 6. Observed failure modes.

$t_{steel} = 10mm$, pultruded CFRP S&P HM(200/2000), and four different adhesives. Two specimens made with rigid adhesives (SIKADUR30 and S&P HP220) and two made with ductile adhesive (AW4858/HW4858 and Araldite 2052–1) are presented in Fig. 7 (a), (b), (c), and (d), respectively. The strains are measured in the Y-Y direction parallel to the loading. Note the DIC contour plots show only half the CFRP length as captured with a DIC camera to achieve sharp focus. Fig. 7 (a) shows the specimen made with SIKADUR 30, where the deformation concentrates near the middle of the joint until covering around 30 % of the CFRP before failure, with the maximum strain that does not reach 0.4 %. The specimen with S&P HP220 adhesive presented in Fig. 7 (b), shows a larger deformed area and deformation levels exceeding 0.4 % which is higher than the specimens with Sikadur 30. At higher loading levels, the strains are not distributed uniformly which may indicate the presence of a weaker zone due to manufacturing imperfections such as voids. The specimen with the AW4858/HW4858, shown in Fig. 7 (c), exhibits deformation covering almost all the face of the CFRP before failure. The ductile adhesive brings through a more uniform distribution which explains the higher strength shown in Section 3.1.

Fig. 8 shows the strain field contour plots on the back face of the

CFRP captured using DIC for specimens made with steel thickness $t_{steel} = 6mm$, pultruded CFRP S&P HM (200/2000), and two different adhesives. Fig. 8 (a) and (b) illustrate the contour plots for specimens made with the ductile adhesive AW4858/HW4858 and the rigid adhesive S&P HP220, respectively. Fig. 9 shows the loading stages in the load–displacement curves corresponding to the contour plots presented in Fig. 8. The specimen DSJ-SP-75–6-AW-1–3 made with the ductile adhesive AW4858/HW4858, shown in Fig. 9 (a) reaches higher values of deformation than DSJ-SP-75–6-SP-1–1 made with the rigid adhesive S&P HP220 shown in Fig. 9 (b). Unlike specimens made with steel thickness $t_{steel} = 10mm$, specimens made with steel thickness $t_{steel} = 6mm$ reach high deformation values at all the CFRP area and even at the end of the overlap. Interestingly, the deformation level at the end of the overlap decrease to zero in step 3 and step 4 where the joints are subjected to large plastic deformations as shown in Fig. 9. This indicates that the debonding starts at the end of the overlap for specimens made with steel thickness $t_{steel} = 6mm$, which is completely different than the behavior observed for specimens with $t_{steel} = 10mm$, where debonding started from the middle.

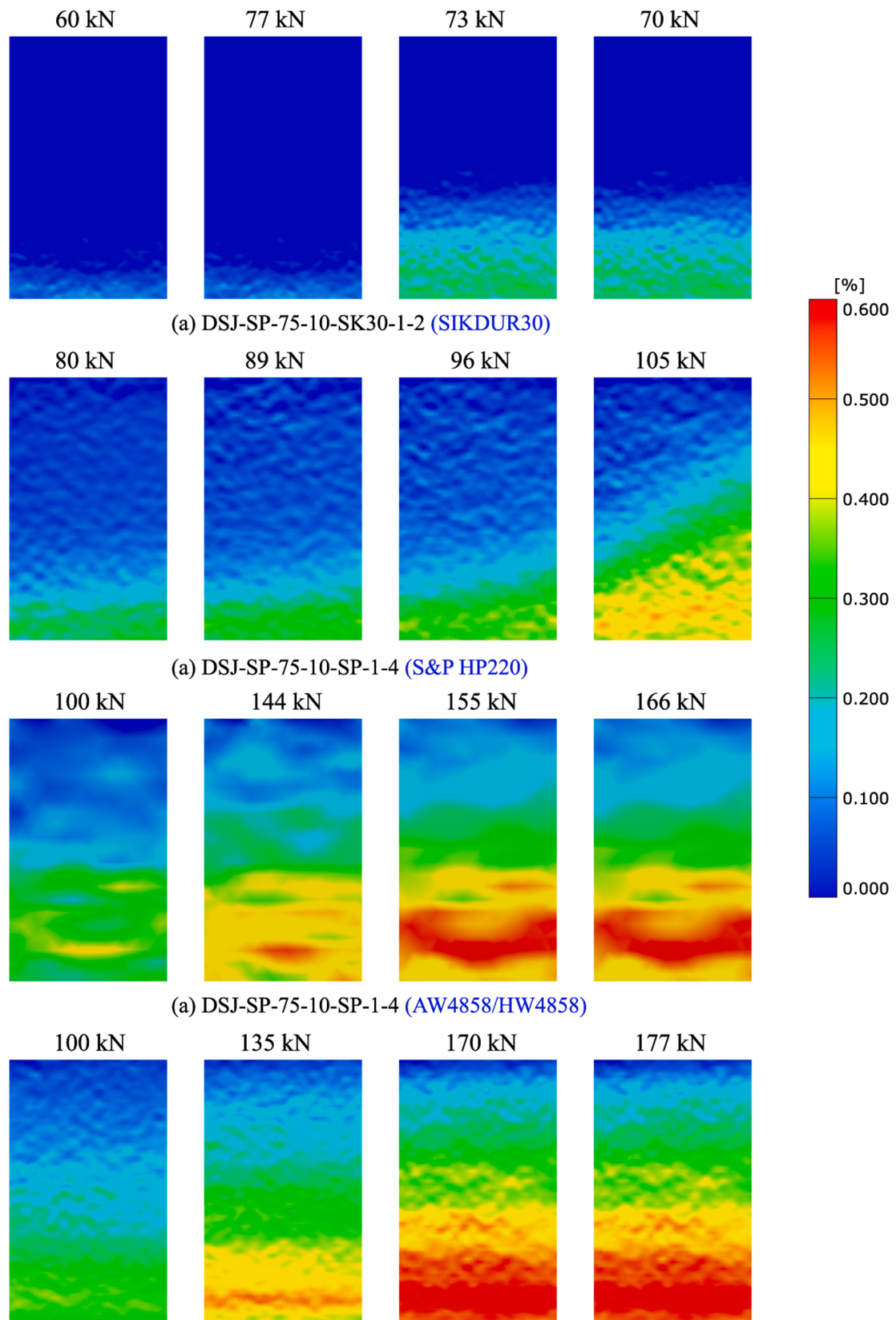**Fig. 7.** Strain fields on the CFRP back face for the double strap joints with the different adhesives (steel thickness 10 mm, pultruded CFRP S&P HM (200/2000), and half CFRP length L = 75 mm).
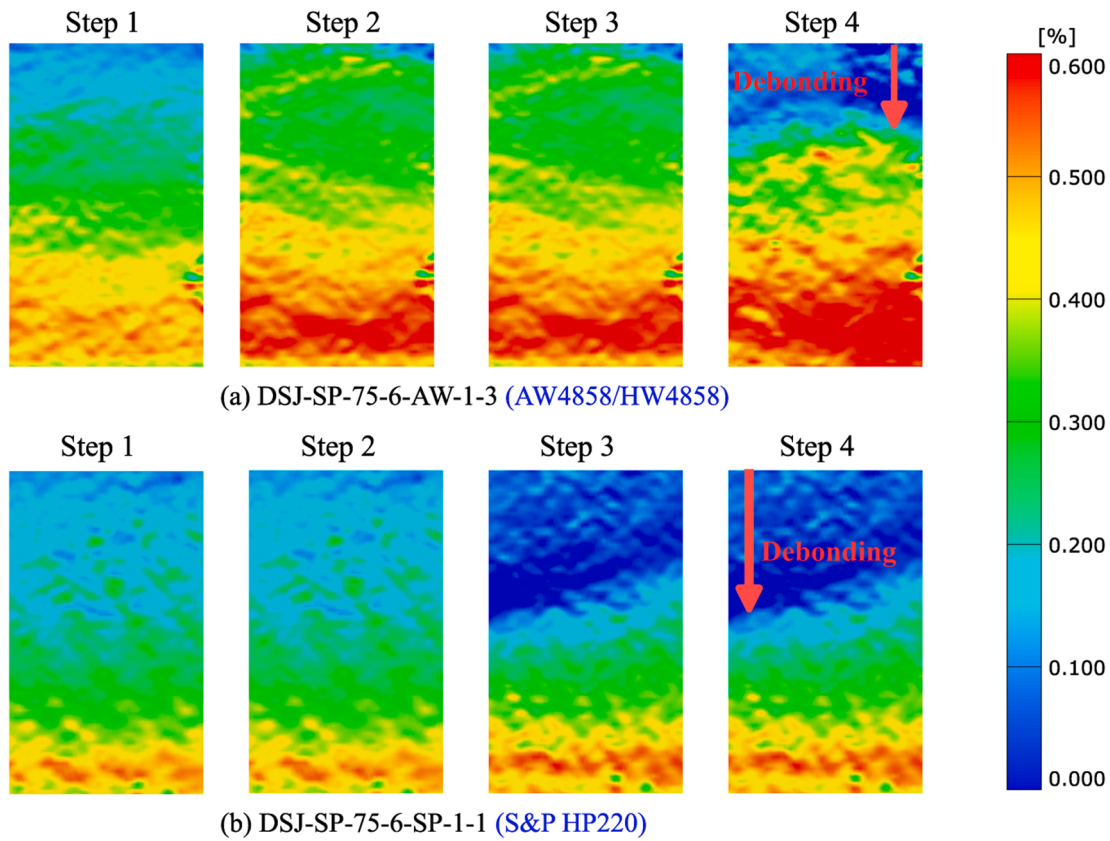
Fig. 8. DIC contour plots on the back face of the CFRP for specimens with steel thickness = 6 mm. (Note: only half of the joint in shown): (a) specimen with ductile adhesive AW4858/HW4858; (b) specimen with rigidi adhesive S&P HP220.
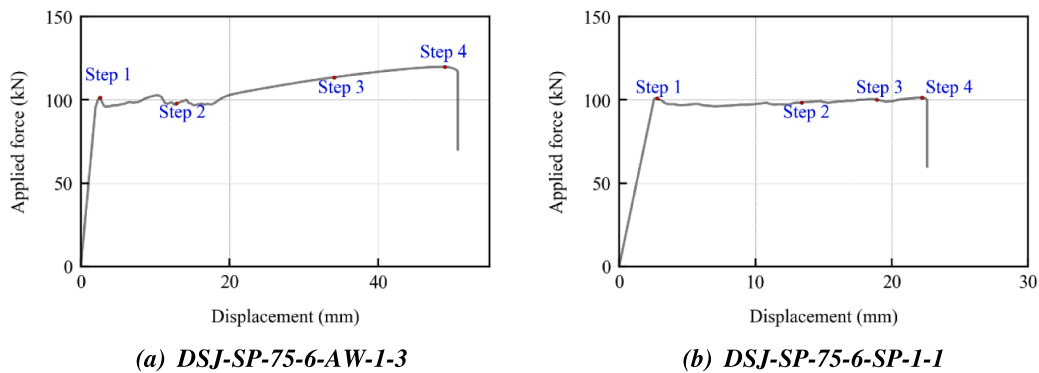

Fig. 9. Load displacement curves showing the loading stage of each DIC contour plot shown in Fig. 8.

4. Numerical analysis

A 2D Finite element model was developed in the commercial software ABAQUS® to simulate the behavior of the DSJ specimens. Specimens made with a steel thickness of $t_{steel} = 10mm$ and $t_{steel} = 6mm$ are modelled for comparison and verify the yielding that was observed in Fig. 5. For the sake of simplicity and brevity, only specimens with one ductile adhesive (i.e. AW4858/HW4858) and one rigid adhesive (i.e. S&P HP220) adhesive are simulated. Note the simulation of cracks in any component of the DSJ joints is beyond the scope of this study. Certain mode of failures such as cohesive failure can be simulated using cohesive zone models [35,36], however, delamination and adhesive failure are more challenging to model. Only specimens with pultruded CFRP laminate are modelled. The numerical model presented in this section is mainly to verify the observations obtained experimentally and

check the distribution of stresses and deformation.

The model is shown in Fig. 10 (a), which consists of a steel bar, adhesive layers, CFRP plates, and testing machine grips. Half of the joint was modelled due to symmetry. Since yielding was observed in the load–displacement curves of some specimens, the machine gripes were also modelled in order to capture any stress concentration zone created by the compression of the grips. The numerical model has the same geometry and dimensions as the experimental specimens used in the experiment with CFRP length equal $L_{CFRP} = 75mm$, adhesive thickness $t_{thickness} = 1mm$, CFRP thickness $t_{CFRP} = 1.4mm$ and the steel bar length $L_{steel} = 500mm$. All the model was developed using plane stress linear quadrilateral elements CPS4R available in the software library. The elastoplastic material behavior of the steel and the adhesives was modelled using an isotropic model calibrated using experimental true stress–strain curves. The parameters used to model the steel behavior
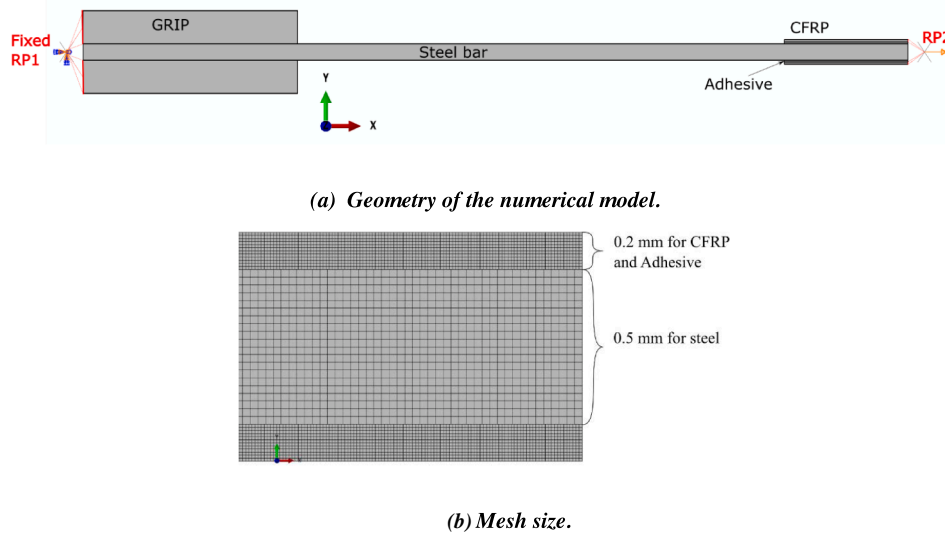
(a) Geometry of the numerical model.

(b) Mesh size.

Fig. 10. Finite element model of DSJ specimens.

and the adhesives are presented in Table 5 and Table 6, respectively. The CFRP has a strong unidirectional behavior following the direction of the fibres, and a weaker behavior in the other directions. Hence, it is more appropriate to model the behavior of the CFRP using an orthotropic material model. The micro-mechanics can be used to predict the anisotropy behavior of CFRP, such as reported in [36,37]. However, due to the unavailability of experimental data, the CFRP plates were assumed isotropic. This assumption is supported who Haghani [38] who investigated the effect of considering orthotropic or isotropic for similar specimens. This assumption is adopted by several research in the literature [19,39–42].

A refined meshing was adopted in the numerical model with a mesh size of $0.5mm$ for the steel bar and $0.2mm$ for the CFRP and adhesive layer, as shown in Fig. 10 (b). A rigid body surface-to-surface tied constraints were assumed between the grips and the steel bar to ensure no slip as in the experiment. A compression force of $1MN$ was uniformly applied on the grips as in the experiment. The material of the grips was assumed as linear steel with an elastic modulus $E = 200GPa$. The free edge of the grips was constrained as a rigid body to a reference point "RP1" which was in turn restrained in all degrees of freedom to ensure fixed boundary conditions. The loading was applied on the CFRP edge section as only half of the joint is modelled. The CFRP edge section was constrained as a rigid body to a reference point RP2 where a displacement loading was imposed. The steel/adhesive interface was modelled with tie constraints where the steel surface is taken as the master surface and the adhesive surface as a slave. Similarly, for the CFRP/adhesive interface, the CFRP surface is taken as master and the adhesive surface as a slave.

Table 5
Steel material elastoplastic model input parameter.

Material	Elasticity		Plasticity	
	Elastic modulus (GPa)	Poisson ratio	Yield stress (MPa)	Plastic strain
Steel ($t\_steel = 10mm$)	200	0.3	350	0
			370	0.022
			440	0.0517
			500	0.1
Steel ($t\_steel = 6mm$)	200	0.3	324	0
			340	0.022
			420	0.0517
			480	0.1

Table 6
Adhesive elastoplastic model input parameters.

Material	Elasticity		Plasticity	
	Elastic modulus (GPa)	Poisson ratio	Yield stress (MPa)	Plastic strain
AW48584/ HW4858	1.32	0.35*	35.5	0
			36	0.15
SP HP220	7.6	0.35*	N.A.	N.A.

* Assumed parameter.

Fig. 11 shows that the numerical results match fairly well the experimental data. The numerical load–displacement curve of the double strap joint made with steel thickness $t_{steel} = 10mm$ and AW4858/HW4858 adhesive representative to experimental specimens "DSJ-SP-75–10-AW-1-repetition No" reach a maximum force of 152kN and then shows a plateau. At this stage of loading, maximum stress is 340 MPa, which represents 97 % of the yield stress. Referring to Fig. 12, the active yield parameter indicates that at this stage the steel did not experience any plastic deformation, but the limited plastic deformation observed in the curve is due to the adhesive plastic behavior, as shown in Fig. 5. Note that the specimen "DSJ-SP-75–10-AW-1-3" that experimentally reached a maximum load of 168kN and developed large ductile behavior, the steel should have yielded likewise specimens with $t_{steel} = 6mm$, which developed large ductile behavior. Fig. 11 (b) shows the behavior of the specimen with S&P HP220 adhesive ($t_{steel} = 10mm$) that experienced only a linear behavior in the steel and the adhesive before the brittle failure that occurred in the experiment.

Fig. 11 (c) and (d) show specimens with $t_{steel} = 6mm$ for both adhesives AW4858/HW4858 and S&P HP220, respectively. The numerical model could successfully capture the nonlinear behavior observed experimentally. The specimens developed mainly significant plastic deformation in the steel bars as shown in Fig. 12. This induced a concentration of deformation at the steel-adhesive interface at the end of the overlap, which can be seen in Fig. 13, for both specimens with the ductile adhesive AW4858/HW4858 or the brittle adhesive S&P HP220. The joint with the ductile adhesive developed a much larger plastic deformation.

From Fig. 14, the behavior of specimens with $t_{steel} = 10mm$ exhibited a different behavior, where the distribution of the logarithmic strain LE11 mainly concentrate in the middle of the joint (i.e. the right side, only half of the joint is modelled). The deformation concentrates mainly near the CFRP-adhesive interface where the minimum negative
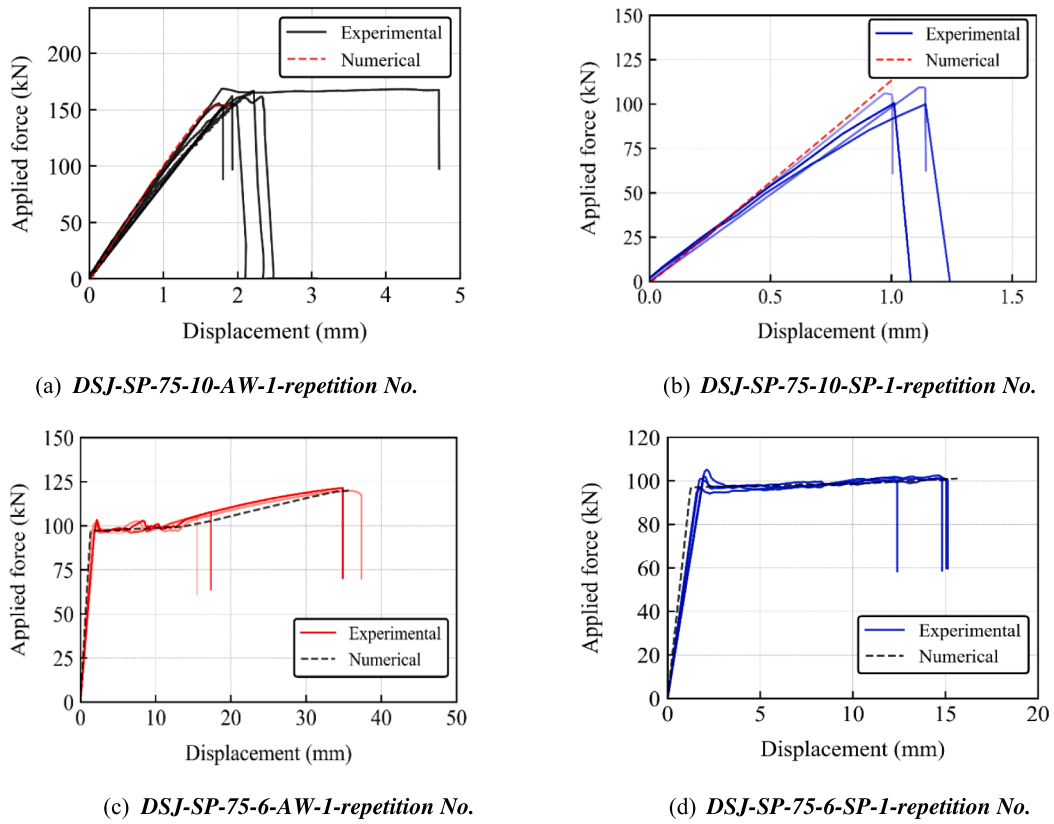
(a) *DSJ-SP-75-10-AW-1-repetition No.*

(b) *DSJ-SP-75-10-SP-1-repetition No.*

(c) *DSJ-SP-75-6-AW-1-repetition No.*

(d) *DSJ-SP-75-6-SP-1-repetition No.*

Fig. 11. Comparison between experimental and numerical results for DSJ specimens with t_{steel} of 10 mm ((a) and (b)) or 6 mm ((c) and (d)), AW4858/HW4858 adhesive ((a) and (c)), and S&P HP220 adhesive ((b) and (d)).
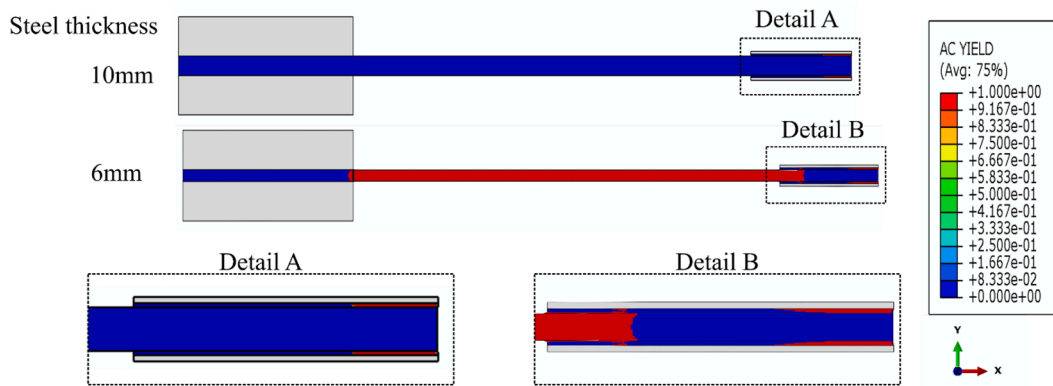

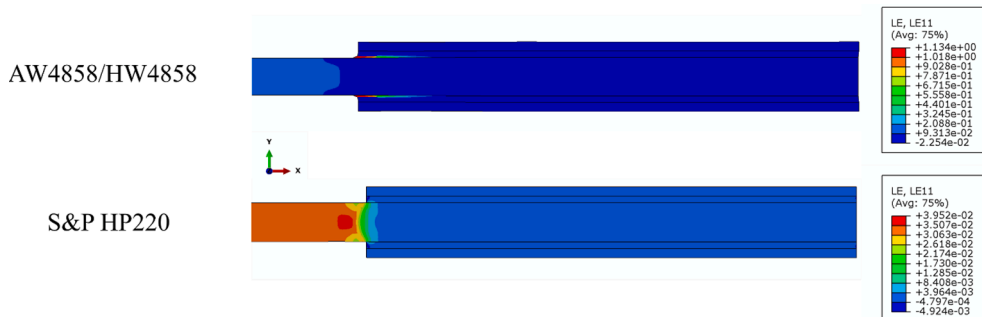**Fig. 12.** Active yielded area for specimens with AW4858/HW4858 adhesive.

Fig. 13. Logarithmic deformation (LE11) in the longitudinal direction(X-X) for specimens made with $t_{steel} = 6mm$.
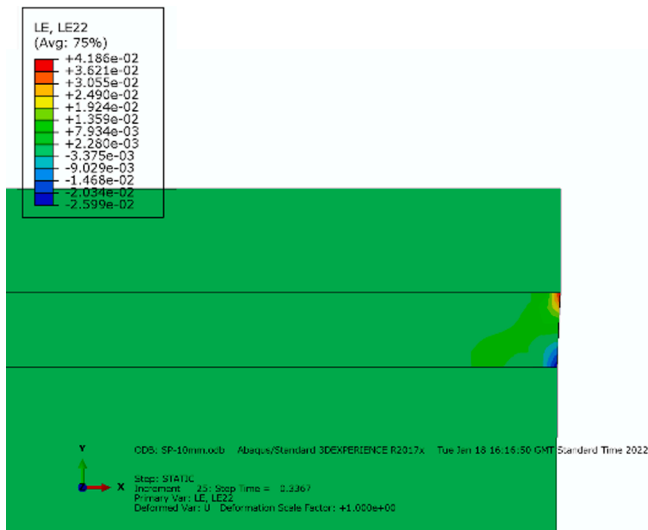
Fig. 14. Peeling deformation LE22 (Y-Y direction) for 10 mm-SP.

deformation is observed in the adhesive layer and the large positive deformation on the CFRP side which leads to very high shear stresses. This is true for both AW4858/HW4858 and S&P HP220 as shown in detail C and detail D in Fig. 15. Whereas near the end of the overlap (e.g. detail B, Fig. 15) the level of deformation is very low. Fig. 14 shows that peeling deformation is also significant near the CFRP-adhesive interface for a specimen with $t_{steel} = 10mm$. The concentration of shear deformation and peeling near the CFRP-adhesive interface at the middle of the joint for specimens with $t_{steel} = 10mm$ make this region the most vulnerable to debonding.

5. Parametric results and discussions

5.1. Influence of the adhesive type

Ductile adhesives (i.e. AW4858/HW4858 (AW) and Araldite 5052–1

(AR)) used in this study have high yielding strength and large deformation capacity which make them extremely tougher than the brittle adhesives (i.e. SIKADUR30 (SK30) and S&P HP220 (S&P)). Fig. 16 indicates that specimens made with ductile adhesives achieved very high strength compared to the ones made with brittle adhesives. Specimens with the brittle adhesive SK30 achieved a mean strength of 76kN with a standard deviation of 5.52kN and specimens with a slightly tougher rigid adhesive (S&P HP220) achieved a mean strength of 105kN with a standard deviation of 3.65kN. Whereas specimens with ductile adhesives AW and AR reached mean strengths of 161kN and 171kN with standard deviations of 5.45kN and 8.6kN, respectively. The difference in performance between ductile adhesives and rigid ones is significant with a mean strength ratio ranging from 1.53 to 2.25. As shown earlier from the DIC results, ductile adhesives promote a more uniform distribution of deformation in the bonded joint which reduces the stress concentration.

It was also observed in section 3.2 that the adhesive type influenced the failure mode. The failure in the CFRP/steel bonded joints is a crack that initiates and propagates in the component that satisfies the Griffith energy criterion $G > G_c$, where G is the energy demand on the material, and G_c is a material property called critical strain energy release rate. The delamination failure mode occurs due to a crack in the CFRP matrix
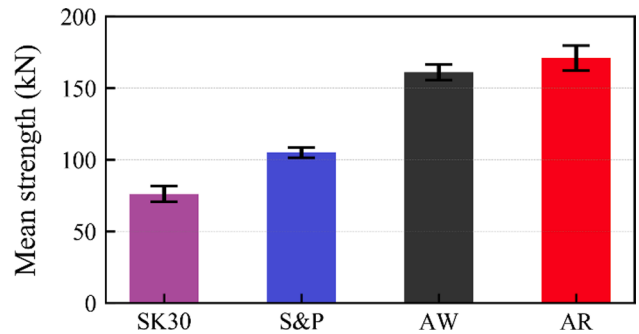

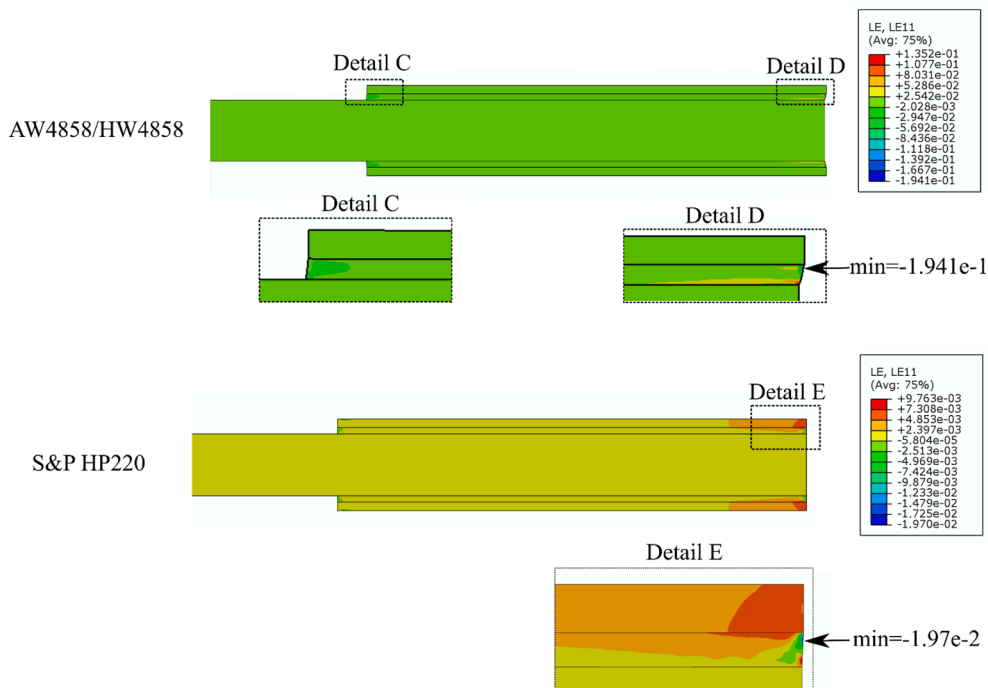Fig. 16. Effect of adhesive type on the DSJ mean strength.

Fig. 15. Logarithmic deformation (LE11) in the longitudinal direction(X-X) for specimens made with $t_{steel} = 10mm$.

and cohesive failure due to a crack in the adhesive layer. For specimens presented in Table 4 "control: Adhesive type", the failure modes were either cohesive or CFRP delamination. When the extremely tough adhesives (ductile) were used, delamination occurred, whereas, for brittle adhesives with lower toughness, cohesive failure occurred. For example, for joints bonded with the adhesive having the lowest toughness (i.e. SK30), cohesive failure governed the failure mode, whereas, for tough ductile adhesives such as AW and AR, CFRP delamination was the failure mode. For specimens with S&P HP220 which is moderately tougher than SK30, a combination of CFRP delamination and limited cohesive failure governed the failure mode.

5.2. Influence of adhesive thickness

The effect of the adhesive thickness on the strength of adhesive joints is a complex and open issue. The adhesive thickness may influence the stress state in the adhesive layer and enlarge the distribution of shear stresses. However, the eccentricity generated by thickness gives rise to higher peeling stress. Besides, larger voids are likely to be present in thicker adhesive bond lines. From a fracture mechanic point of view, researchers gave conflicting conclusions, while some researchers [43] suggested that with decreasing adhesive thickness, the fracture energy reduces significantly, others [44] observed that the adhesive thickness influences the fracture process zone shape (FPZ) causing the adhesive joint fracture to behave differently where thinner adhesive bond lines lead to a stretched thin FPZ, delaying the crack propagation. From Table 4, specimens with S&P HP220 adhesive with 1 mm thickness failed under delamination dominant failure mode whereas specimens with 0.6 mm failed under cohesive dominant failure mode. This can be seen in Fig. 4(c) and 4(d) which illustrate a specimen with a thin layer (0.6 mm) that failed under cohesive dominant failure mode and a thicker layer (1 mm) under delamination dominant failure mode. In this study, specimens made with SP and AW adhesives were tested with three different thicknesses (i.e. 0.6 mm, 1 mm, 1.6 mm) for comparison, as shown in Table 4 "control: Adhesive thickness". Fig. 17 (a) shows the variation of mean strength for specimens made with S&P HP220 adhesive. The strength fluctuates and the results are not conclusive. This has been also observed in the experiments of Yu et al. [7] for specimens with a brittle adhesive. Fig. 17 (b) shows that the joint strength decreases with the increase of the adhesive thickness.

5.3. Influence of CFRP modulus

Two normal modulus pultruded CFRP, namely: CFRP (SIKA Carbodure S512, $E = 160 GPa$) and (S&P HM 200/2000, $E = 205 GPa$) and one high modulus wet lay-up laminates made with CFRP sheets (S&P C-Sheet 640, $E = 640 GPa$) were used in this study. Joints with high modulus CFRP could achieve very high strength when bonded with ductile tough adhesives AW. Specimens with high modulus CFRP and $t_{steel} = 10 mm$ achieved a very high strength with values of 161.3 kN and

173.3 kN which is quite similar to the ones made with the normal modulus where the strength varied between 155.5 kN and 168 kN. Specimens with high modulus CFRP and $t_{steel} = 6 mm$ achieved the yield strength and developed a ductile behavior for specimens with the pultruded CFRP. However, the fracture behavior of the joints with two types of CFRP is different. For joints with high modulus CFRP, a rupture of CFRP in the middle of the joint occurred which is mainly due to the low deformation capacity of the high modulus CFRP. Whereas joints with normal modulus CFRP, delamination failure occurred. The normal modulus pultruded CFRP S512 was used to make only 2 specimens. This was made only for the sake of comparison with the pultruded CFRP S&P HM200/2000 that was used in most specimens. The results revealed that the specimens with CFRP S512 achieved higher strength than the ones made with CFRP S&P HM20/2000 with averages of 119.15 kN and 105 kN, respectively. This can be justified by the fact that the CFRP S512 has a higher strength and higher deformation capacity.

5.4. Effect of CFRP length

Fig. 18 (a) and (b) illustrate the variation of the mean strength with respect to the CFRP length for specimens with S&P HP220 adhesive and AW adhesive, respectively. Clearly, the mean strength increases with the increase in the CFRP length. Note a maximum length of $L = 75 mm$ was used in this study. Longer CFRP may lead to an increase of strength until reaching a limit where no further increase can be reached. Usually, the CFRP length corresponding to this limit is called the effective length in the literature [10]. However, the determination of the effective bond length is beyond the scope of this study. The CFRP length considered here is intended to represent a repair patch in cracked structural details such as in the case of connections where limited space is available for longer CFRP.

5.5. Effect of steel thickness

DSJ Specimens with $t_{Steel} = 6 mm$ and $t_{steel} = 10 mm$ were tested for comparison of the behavior. Due to the lower yield strength of steel bars with $t_{steel} = 6 mm$, the DSJ specimens developed large plastic deformation before failure. Numerical results revealed that the plastic deformation occurred mainly in the steel bars outside the joint region. The DIC results showed that the yielding of the steel bars influences the strain distribution on the CFRP back face and the failure pattern. For specimens with $t_{steel} = 6 mm$ made with the rigid adhesive SP HP220 "DSJ-SP-75–6-SP-1-repetition No.", the failure mode was mainly in the steel-adhesive interface due to the large plastic deformation that occurred in the steel. Specimens made with the ductile adhesive did not fail in the steel-adhesive interface due to the high ductility of the adhesive. Most specimens with $t_{steel} = 10 mm$ did not develop plastic deformation in the steel and failure was generated from the gap region in the middle of the joint.

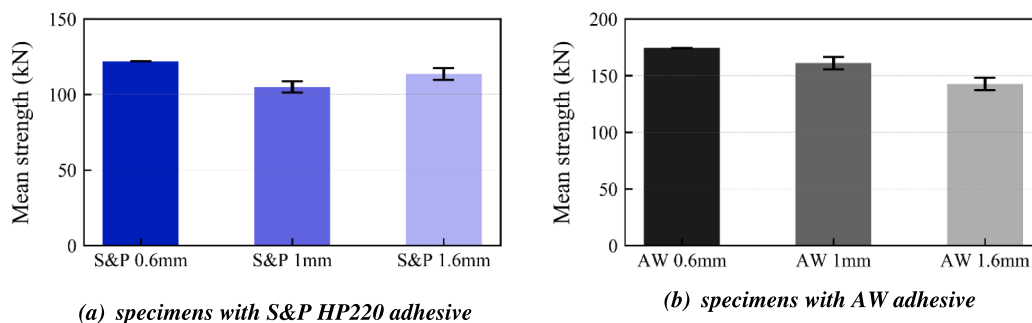Although steel yielding is usually avoided in the experimental studies

(a) specimens with S&P HP220 adhesive

(b) specimens with AW adhesive

Fig. 17. Effect of adhesive thickness on the mean strength of DSJ specimens. Note: The thickness of the adhesive (i.e. 0.6 mm, 1 mm, or 1.6 mm) of each joint type is presented in the bar charts.
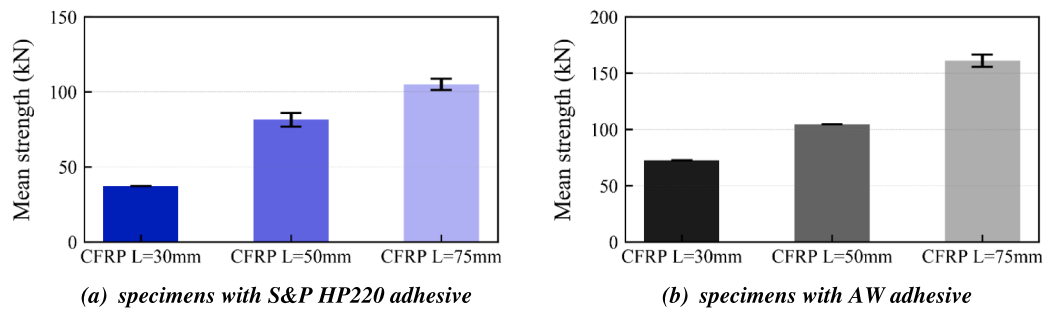
(a) specimens with S&P HP220 adhesive

(b) specimens with AW adhesive

Fig. 18. Effect of CFRP length on the mean strength of DSJ specimens.

in the literature [7] by using thick rigid steel blocks instead of using double strap joints with relatively thin bars. However, the steel thickness influence significantly the behavior of adhesively bonded joints, which can change completely the distribution of stress and the failure mode. Therefore, it is important to use steel elements with thicknesses representative of practical situations. For example, $t_{steel} = 6-10mm$ can be found in old metallic bridges, which was the main reason for the choice of thicknesses used in this study.

5.6. Surface treatment

The surface treatment is a very important step for the successful bonding of the adhesive joint. As stated previously, sandblasting with alumina dioxide grain size between 212 and 300 μm, used in this study, is the most recommended method [12]. However, for acrylic-based structural adhesive Araldite 2052–1, the manufacturer claims in the datasheet that no or little surface preparation is required for perfect bonding. This can facilitate significantly, the implementation of this technology in practice. So in this study, four DSJ joints were tested with Araldite 2052–1, wherein in two of them the steel was sandblasted (i.e. DSJ-SP-75–10-AR-1-"repetition 1 and 2"), and in two the steel was only polished using an angle grinder with sand-paper grit 80 (i.e. DSJ-SP-75–10-AR-1-"repetition 3 and 4"). As shown in Table 4, the results revealed that the specimens polished only with sandpaper achieved a very high strength of 175.1kN and 175.3kN and specimens with sand blasting achieved 156.2kN and 177.5kN. It can be concluded that the adhesive Araldite 2052–1 requires very low surface preparation which can be very useful in practical situations.

5.7. Discussion on failure modes

Usually, it is assumed that a well-designed adhesive joint will fail cohesively. This might be true in the case of very tough adherends such as in metal–metal adhesively bonded joints. However, using extremely tough adhesives such as the ones used in this study render the cohesive failure not possible in a CFRP joint. The pultruded CFRP available in the market is usually made with vinyl ester adhesives which have lower toughness than the extremely tough ductile adhesives. The CFRP inter-laminar toughness may be increased by using tougher adhesive in the impregnation however, the concentration of deformation in the adhesive-CFRP interface at the middle of the joint as shown in Fig. 15 favour a delamination failure since the first CFRP layers in the laminate will be subjected to high shear stress and peeling stress.

Specimens with lower steel thickness are likely to experience steel yielding then a failure in the adhesive-steel interface will start from the end of the overlap. Note this failure mode is not a premature failure due to inadequate surface treatment. The authors believe that this the most suitable failure mode for adhesive joints because the joint develop very large ductility in the steel before failure and more importantly, this means that the CFRP adhesive joint is stronger than the yield strength of the parent material.

6. Joint strength efficiency for the design of steel/CFRP adhesively bonded joints

As shown throughout this study, CFRP-steel adhesive joints achieve very high strength when bonded with ductile tough adhesives. Some specimens with $t_{steel} = 10mm$ and all specimens with $t_{steel} = 6mm$ developed a ductile behavior in the steel part. As stated previously, this is the most suitable failure mode for CFRP/steel adhesive joints since it means that the adhesive joint is stronger than the yield strength of the parent steel structural detail. In that sense, if the yield strength of the parent material (steel) can be used as a design parameter of the adhesively bonded joints, similarly to the joint efficiency used for welded joints which refers to the strength ratio of the joint with respect the strength of the base metal, the design of adhesive joints can become much simpler. A Joint Efficiency of 100 % indicates that the joint has the same strength as the base metal and can be used confidently in practical situations. This design parameter would help to avoid cumbersome design checks on the fracture of the adhesive layer or the CFRP, which are very complex. So further development of design rules based on joint efficiency is higher recommended in future research.

7. Conclusion

This study focused on the characterization of CFRP/Steel adhesively bonded joints. For this purpose, experimental and numerical analyses were conducted on CFRP/steel double strap joints including several variants such as the adhesive type, steel thickness, CFRP modulus, CFRP length, adhesive thickness, and surface preparation. The results revealed that:

- Steel/CFRP joints with ductile (tough) adhesives achieve much higher strength than the ones made with rigid adhesives commonly used in construction practice. The failure modes for specimens made with rigid adhesive are mainly a combination of cohesive and CFRP delamination failure, whereas in the joints made with ductile adhesive only CFRP delamination occurred. The CFRP/steel joints with ductile adhesives did not fail under cohesive mode due to the high toughness of the adhesive compared to the one used for CFRP impregnation.
- When steel yielding occurs in the part outside of the joint region, the joint develops a ductile behavior, and the distribution of stress in the adhesive bond line changes. Stress concentration becomes significant at the end of the overlap in the steel/adhesive interface. Joints with brittle adhesive showed an adhesive failure mode at the steel/adhesive interface, whereas ductile adhesive sustained large plastic deformation and failed under CFRP delamination.
- For joints with ductile adhesive, an increase in adhesive thickness was associated with a decrease in strength. Whereas specimens with rigid adhesive the results fluctuated, and the influence could not be observed.

- Joints with both normal modulus CFRP and high modulus CFRP achieved very high strength when bonded with a ductile adhesive. DSJ specimens with high modulus CFRP failed under CFRP rupture in the middle and joints with normal modulus CFRP, exhibited CFRP delamination mode.
- DSJ specimens with the acrylic-based adhesive that received low-quality of surface treatment (angle grinder sandpaper) achieved very high strength similar to the ones prepared with sandblasting.
- The joint efficiency methodology used for welded connection is recommended for adhesively bonded joints for future research to develop certified composite patches ready to be used in practice.

CRediT authorship contribution statement

Anis Mohabeddine: Validation, Conceptualization, Data curation, Formal analysis, Investigation, Methodology, Writing – original draft. **Ghassan Malik:** Execution of the study, Data analysis. **José Correia:** Data analysis, Writing, Validation, Supervision. **Filipe Silva:** Investigation, Methodology. **Abílio De Jesus:** Funding acquisition, Supervision, Writing – review & editing. **Nicholas Fantuzzi:** Validation, Supervision, Writing – review & editing. **José Miguel Castro:** Validation, Supervision.

Declaration of Competing Interest

The authors declare that they have no known competing financial interests or personal relationships that could have appeared to influence the work reported in this paper.

Data availability

Data will be made available on request.

References

[1] Mohabeddine A, Correia JAFO, Montenegro PA, Castro JM. Fatigue crack growth modelling for cracked small-scale structural details repaired with CFRP. Thin-Walled Struct 2021;161:107525.

[2] Kasper Y, Albiez M, Ummenhofer T, Mayer C, Meier T, Choffat F, et al. Application of toughened epoxy-adhesives for strengthening of fatigue-damaged steel structures. Constr Build Mater 2021;275:121579.

[3] Mohabeddine A, Correia J, Montenegro PA, De Jesus A, Castro JM, Calçada R, et al. An approach for predicting fatigue life of CFRP retrofitted metallic structural details. Int J Fatigue 2022;154:106557.

[4] Mohabeddine A, Correia J, Aires Montenegro P, De Jesus A, Miguel Castro J, Berto F. Probabilistic S-N curves for CFRP retrofitted steel details. Int J Fatigue 2021;148:106205.

[5] Mohabeddine A, Correia JAFO, Castro JM, Montenegro P, De Jesus AMP, Calçada RAB. Numerical investigation on the fatigue life of non-cracked metallic plates repaired with bonded CFRP. ce papers 2021;4(2-4):1135–44.

[6] Naboulsi S, Mall S. Modeling of a cracked metallic structure with bonded composite patch using the three layer technique. Compos Struct Jul. 1996;35(3):295–308. https://doi.org/10.1016/0263-8223(96)00043-8.

[7] Yu T, Fernando D, Teng JG, Zhao XL. Experimental study on CFRP-to-steel bonded interfaces. Compos Part B Eng 2012;43(5):2279–89. https://doi.org/10.1016/j.compositesb.2012.01.024.

[8] Russian O, Khan S, Belarbi A, Dawood M. Effect of surface preparation technique on bond behavior of CFRP-steel double-lap joints: Experimental and numerical studies. Compos Struct Jan. 2021;255:113048. https://doi.org/10.1016/j.compstruct.2020.113048.

[9] Xia SH, Teng JG. Behavior of FRP to Steel Bonded Joint. In: *Proceeding of the International Symposium on Bon Behaviour of FRP in Structures (BBFS 2005)*; Jan. 205AD. p. 411–8, [Online]. Available: http://espace.library.uq.edu.au/view/UQ:376041.

[10] Fawzia S, Zhao XL, Al-Mahaidi R. Bond-slip models for double strap joints strengthened by CFRP. Compos Struct 2010;92(9):2137–45. https://doi.org/10.1016/j.compstruct.2009.09.042.

[11] Wu C, Zhao X, Duan WH, Al-Mahaidi R. Bond characteristics between ultra high modulus CFRP laminates and steel. Thin-Walled Struct 2012;51:147–57. https://doi.org/10.1016/j.tws.2011.10.010.

[12] Fernando D, Teng JG, Yu T, Zhao X. Preparation and Characterization of Steel surfaces for Adhesive Bonding. 04013012 1–10 J. Compos. Constr. 2013;17(6). https://doi.org/10.1061/(ASCE)CC.1943-5614.

[13] Silva MAG, Biscaia H, Ribeiro P. On factors affecting CFRP-steel bonded joints. Constr Build Mater 2019;226:360–75. https://doi.org/10.1016/j.conbuildmat.2019.06.220.

[14] Wu C, Zhao X-L, Al-Mahaidi R, Emdad MR, Duan W. Fatigue Tests of Cracked Steel Plates Strengthened with UHM CFRP Plates. Adv Struct Eng Oct. 2012;15(10):1801–15. https://doi.org/10.1260/1369-4332.15.10.1801.

[15] Ke Lu, Li C, Luo N, He J, Jiao Y, Liu Y. Enhanced comprehensive performance of bonding interface between CFRP and steel by a novel film adhesive. Compos Struct 2019;229:111393.

[16] Li C, Ke L, He J, Chen Z, Jiao Y. Effects of mechanical properties of adhesive and CFRP on the bond behavior in CFRP-strengthened steel structures. Compos Struct Mar. 2019;211:163–74. https://doi.org/10.1016/j.compstruct.2018.12.020.

[17] Wang Z, Li C, Sui L, Xian G. Effects of adhesive property and thickness on the bond performance between carbon fiber reinforced polymer laminate and steel. Thin-Walled Struct 2021;158(September 2020). https://doi.org/10.1016/j.tws.2020.107176.

[18] Fawzia S, Al-Mahaidi R, Zhao X. Experimental and finite element analysis of a double strap joint between steel plates and normal modulus CFRP. Compos Struct Sep. 2006;75(1–4):156–62. https://doi.org/10.1016/j.compstruct.2006.04.038.

[19] Jimenez-Vicaria JD, Pulido MDG, Castro-Fresno D. Influence of carbon fibre stiffness and adhesive ductility on CFRP-steel adhesive joints with short bond lengths. Constr Build Mater 2020;260:119758. https://doi.org/10.1016/j.conbuildmat.2020.119758.

[20] Yang Y, Biscaia H, Chastre C, Silva MAG. Bond characteristics of CFRP-to-steel joints. J Constr Steel Res 2017;138:401–19. https://doi.org/10.1016/j.jcsr.2017.08.001.

[21] He J, Xian G. Debonding of CFRP-to-steel joints with CFRP delamination. Compos Struct 2016;153:12–20. https://doi.org/10.1016/j.compstruct.2016.05.100.

[22] Pang Y, Wu G, Su ZL, He XY. Experimental study on the carbon-fiber-reinforced polymer–steel interfaces based on carbon-fiber-reinforced polymer delamination failures and hybrid failures. Adv Struct Eng 2020;23(11):2247–60. https://doi.org/10.1177/1369433220911167.

[23] He J, Xian G, Zhang YX. Numerical modelling of bond behaviour between steel and CFRP laminates with a ductile adhesive. Int J Adhes Adhes 2021;104:102753. https://doi.org/10.1016/j.ijadhadh.2020.102753.

[24] Sika, "Pioneering Steel Bridge Repair: SIKADUR®-370." https://www.sika.com/en/innovation/sika-innovation-flash/pioneering-steel-bridge-repair–sikadur–370.html.

[25] Marques JB, Barbosa AQ, da Silva CI, Carbas RJC, da Silva LFM. An overview of manufacturing functionally graded adhesives – Challenges and prospects. J Adhes Jan. 2019;97(2):172–206. https://doi.org/10.1080/00218464.2019.1646647.

[26] Jesus AMPd, Silva ALLd, Figueiredo MV, Correia JAFO, Ribeiro AS, Fernandes AA. Strain-life and crack propagation fatigue data from several Portuguese old metallic riveted bridges. Eng Fail Anal 2011;18(1):148–63.

[27] Marques EAS, da Silva LFM. Joint strength optimization of adhesively bonded patches. J Adhes 2008;84(11):915–34. https://doi.org/10.1080/00218460802505275.

[28] Chalkley P, Wang C, Baker A. Fatigue Testing of Generic Bonded Joints. In: Advances in the Bonded Composite Repair of Metallic Aircraft Structure. Elsevier; 2002. p. 103–26.

[29] ASTM-D638-14. Standard Test Method for Tensile Properties of Plastics. *ASTM Stand* 2014;08:1–15.

[30] SIKA, "Sika Carbodure S," https://gcc.sika.com/en/construction/refurbishment/structural-strengthening/sika-carbodur-s.html.

[31] S&P Reinforcements, "Technical datasheet C laminates." [Online]. Available: https://www.sp-reinforcement.eu/sites/default/files/field_product_col_doc_file/r_c-laminates_pub_tds_prod_c-laminates_v4.102020_eu_en.pdf.

[32] Clarke JL. EUROCOMP: Structural Design of Polymer composites. London: Chapman & Hall; 1996.

[33] Zhao XL, Zhang L. State-of-the-art review on FRP strengthened steel structures. Eng Struct 2007;29(8):1808–23. https://doi.org/10.1016/j.engstruct.2006.10.006.

[34] Majidi HR, Razavi SMJ, Berto F. Failure assessment of steel/CFRP double strap joints. Metals (Basel) 2017;7(7):1–16. https://doi.org/10.3390/met7070255.

[35] Xin H, Mosallam A, Liu Y, Xiao Yi, He J, Wang C, et al. Experimental and numerical investigation on in-plane compression and shear performance of a pultruded GFRP composite bridge deck. Compos Struct 2017;180:914–32.

[36] Xin H, Mosallam A, Liu Y, Wang C, Zhang Y. Analytical and experimental evaluation of flexural behavior of FRP pultruded composite profiles for bridge deck structural design. Constr Build Mater 2017;150:123–49. https://doi.org/10.1016/j.conbuildmat.2017.05.212.

[37] Xin H, Liu Y, Mosallam AS, He J, Du A. Evaluation on material behaviors of pultruded glass fiber reinforced polymer (GFRP) laminates. Compos Struct 2017;182:283–300. https://doi.org/10.1016/j.compstruct.2017.09.006.

[38] Haghani R. Finite element modelling of adhesive bonds joining fibre-reinforced polymer (FRP) composites to steel. In: Rehabilitation of Metallic Civil Infrastructure Using Fiber Reinforced Polymer (FRP) Composites, Chalmers U. Sweden: Elsevier; 2014. p. 60–95.

[39] Al-zubaidy H, Al-mahaidi R, Zhao X. Finite element modelling of CFRP / steel double strap joints subjected to dynamic tensile loadings. Compos Struct 2013;99:48–61. https://doi.org/10.1016/j.compstruct.2012.12.003.

[40] Al-mosawe A, Al-mahaidi R, Zhao X. Bond behaviour between CFRP laminates and steel members under different loading rates. Compos Struct 2016;148:236–51. https://doi.org/10.1016/j.compstruct.2016.04.002.

[41] Li H, Xu S, Zhang Z, Song C. Experimental and numerical investigation on the corrosion effects on the bonding behavior between CFRP and steel. Compos Struct 2021;259(December 2020). https://doi.org/10.1016/j.compstruct.2020.113465.

[42] Yang Y, Zhao J, Zhang S, Chastre C, Biscaia H. Effect of mechanical anchorage on the bond performance of double overlapped CFRP-to-steel joints. Compos. Struct. 2021;267(November 2020). https://doi.org/10.1016/j.compstruct.2021.113902.

[43] Yuan H, Xu Y. Computational fracture mechanics assessment of adhesive joints. Comput Mater Sci 2008;43(1):146–56. https://doi.org/10.1016/j.commatsci.2007.07.053.

[44] Chaves FJP, Da Silva LFM, De Moura MFSF, Dillard DA, Esteves VHC. Fracture mechanics tests in adhesively bonded joints: A literature review. J Adhes 2014;90(12):955–92. https://doi.org/10.1080/00218464.2013.859075.